Engineering 8 (2022) 138–147

Contents lists available at ScienceDirect

Engineering

journal homepage: www.elsevier.com/locate/eng

Research
Green Chemical Engineering—Article

A General Strategy for Efficiently Constructing Multifunctional Cluster Fillers Using a Three-Fluid Nozzle Spray Drying Technique for Dental Restoration

Dan-Lei Yang [a,b], Dan Wang [a,b], Hao Niu [a,b], Rui-Li Wang [c], Mei Liu [d], Fei-Min Zhang [d], Jie-Xin Wang [a,b,*], Mei-Fang Zhu [c]

[a] State Key Laboratory of Organic–Inorganic Composites, Beijing University of Chemical Technology, Beijing 100029, China
[b] Research Center of the Ministry of Education for High Gravity Engineering and Technology, Beijing University of Chemical Technology, Beijing 100029, China
[c] State Key Laboratory for Modification of Chemical Fibers and Polymer Materials, College of Materials Science and Engineering, Donghua University, Shanghai 201620, China
[d] Jiangsu Key Laboratory of Oral Diseases, Department of Prosthodontics, Affiliated Hospital of Stomatology, Nanjing Medical University, Nanjing 210029, China

ARTICLE INFO

Article history:
Received 12 January 2021
Revised 28 February 2021
Accepted 19 March 2021
Available online 20 August 2021

Keywords:
Multifunctional cluster fillers
Three-fluid nozzle spray drying
Mechanical properties
Antibacterial activity
Radiopacity
Dental resin composites

ABSTRACT

Multifunctional fillers are greatly required for dental resin composites (DRCs). In this work, a spray dryer with a three-fluid nozzle was applied for the first time to construct high-performance complex nanoparticle clusters (CNCs) consisting of different functional nanofillers for dental restoration. The application of a three-fluid nozzle can effectively avoid the aggregation of different nanoparticles with opposite zeta potentials before the spray drying process in order to construct regularly shaped CNCs. For a SiO_2–ZrO_2 binary system, the SiO_2–ZrO_2 CNCs constructed using a three-fluid nozzle maintained their excellent mechanical properties ((133.3 ± 4.7) MPa, (8.8 ± 0.5) GPa, (371.1 ± 13.3) MPa, and (64.5 ± 0.7) HV for flexural strength, flexural modulus, compressive strength, and hardness of DRCs, respectively), despite the introduction of ZrO_2 nanoparticles, whereas their counterparts constructed using a two-fluid nozzle showed significantly decreased mechanical properties. Furthermore, heat treatment of the SiO_2–ZrO_2 CNCs significantly improved the mechanical properties and radiopacity of the DRCs. The DRCs containing over 10% mass fraction ZrO_2 nanoparticles can meet the requirement for radiopaque fillers. More importantly, this method can be expanded to ternary or quaternary systems. DRCs filled with SiO_2–ZrO_2–ZnO CNCs with a ratio of 56:10:4 displayed high antibacterial activity (antibacterial ratio > 99%) in addition to excellent mechanical properties and radiopacity. Thus, the three-fluid nozzle spray drying technique holds great potential for the efficient construction of multifunctional cluster fillers for DRCs.

1. Introduction

The rapid development of nanotechnology is facilitating the exploration and application of nanomaterials in novel tools for a wide variety of applications, such as energy [1], catalysts [2], electronics [3,4], biomedicine [5–7], and the environment [8]. In particular, the biomedical applications of nanomaterials have attracted broad attention due to the unique and advantageous properties of such materials. Nowadays, dental cavities are one of the most common oral diseases. Tooth decay results in the formation of cavities in the teeth, and the enamel cannot regenerate once it becomes worn or eroded [9]. Without effective treatment, caries can progress until the teeth are destroyed [10]. Hence, reliable and versatile restoration materials are greatly required. Resin composites have been widely used in recent years for treating dental caries due to their numerous advantages, such as esthetics, biocompatibility, mechanical properties, and operability [11].

The main components in dental resin composites (DRCs) are organic matrices and inorganic fillers. The organic matrices, which mainly comprise polymerizable monomers and photoinitiators, can be converted from a liquid phase into a highly crosslinked polymer by being exposed to visible light [12]. Different inorganic fillers have various functions, such as enhancing mechanical properties, reducing polymerization shrinkage, altering thermal expansion behavior, and endowing DRCs with remineralization,

* Corresponding author.
E-mail address: wangjx@mail.buct.edu.cn (J.-X. Wang).

https://doi.org/10.1016/j.eng.2021.08.001

radiopacity, and antibacterial abilities [13–16]. The type, size, shape, and structure of the inorganic fillers are the decisive factors in establishing the properties of DRCs [17–21].

The most commonly used inorganic fillers are reinforcing fillers, such as SiO_2 and glasses, which are essential for nearly all commercial DRCs. These hard and chemically inert fillers are dispersed in organic matrices to provide the necessary structural reinforcement for clinical applications [22]. Although DRCs loaded with reinforcing fillers have been widely used to treat dental caries, secondary caries cannot be avoided at the tooth-restoration interfaces; this is one of the major reasons for restoration failure and results in 50%–70% failed restorations out of all restorations that are placed [23]. Therefore, antibacterial materials, such as fluorides, silver (Ag)-related fillers, and ZnO nanoparticles, have been adopted as co-fillers to give DRCs antibacterial activity [24–26]. Furthermore, dental clinics require DRCs to have radiopacity, which allows dentists to easily differentiate a restoration from a decayed tooth, evaluate voids, identify inappropriate contour in restorations, and diagnose secondary caries around the restorations [27]. Radiopacity can be achieved by incorporating an element with a relatively high atomic weight (e.g., Zr, Sr, or Ba) as the co-filler in DRCs [28]. According to the various requirements for DRCs, fillers with different functions must be embedded into DRCs to achieve multifunctional restorations. However, the direct addition of functional co-fillers may detrimentally affect the mechanical properties of DRCs due to incompatibility between the fillers and resin matrices [26,29,30].

Aside from filler type, filler structure is a crucial factor in determining the mechanical properties of DRCs [17,31,32]. Recent research has demonstrated that nanoparticle clusters (NCs) have a superior reinforcing effect, and NCs have been applied in commercial DRCs (e.g., Filtek Z350 XT, 3 M ESPE, USA). Several methods, including coupling [33], sintering [34], and solvent evaporation [35], have been used to prepare NCs as fillers for DRCs. However, to the best of our knowledge, few of these processes have been applied to construct NCs with more than one component.

Spray drying is an efficient and robust particle-production method that has been widely used in industrial processes [36], such as in the food [37], pharmaceutical [38], and chemical [39,40] industries. It enables the continuous and fast production of particles within a reasonable size range. In our previous work, SiO_2 NCs (SNCs) [41], hydroxyapatite (HAp) NCs [42], and SiO_2–ZnO complex NCs (CNCs) [43] were precisely constructed using a spray dryer with a two-fluid nozzle. The DRCs filled with these NCs showed significantly enhanced properties compared with those filled with the nanoparticle counterparts. In particular, DRCs filled with the SiO_2–ZnO CNCs displayed enhanced antibacterial activity while maintaining good mechanical properties [43]. However, their lack of radiopacity makes such DRCs unsuitable for clinical applications.

Our objective in the present work is to provide a general strategy to construct multifunctional fillers for DRCs using a spray dryer with a three-fluid nozzle. The use of a three-fluid nozzle avoids the aggregation of incompatible particles before the spray drying process, which may occur with the use of a traditional two-fluid nozzle due to its single feed line and nozzle [44,45]. In general, three-fluid nozzle spray drying has been applied in biomedicines, especially for microencapsulation [46–48]. Herein, we report on the use of the three-fluid nozzle spray drying process for the first time in the construction of multifunctional CNCs. ZrO_2 and ZnO nanoparticles were adopted as the co-fillers of SiO_2 nanoparticles in order to realize radiopaque and antibacterial properties in the DRCs. The filling properties of the CNCs constructed by two- and three-fluid nozzles were compared. In addition, a heat treatment process was applied to strengthen the structure of the CNCs. The relationships between the SiO_2–ZrO_2 ratios in the heat-treated CNCs and the properties of the DRCs were investigated. The radiopacity and antibacterial activity of the DRCs filled with SiO_2–ZrO_2–ZnO CNCs were confirmed. The universality of three-fluid nozzle spray drying was also explored.

2. Experimental section

2.1. Reagents and materials

Absolute ethyl alcohol (C_2H_5OH), tetraethyl orthosilicate (TEOS), ammonium hydroxide ($NH_3{\cdot}H_2O$), sodium hydroxide (NaOH), *n*-propylamine, and cyclohexane were bought from Beijing Chemical Reagent Co., Ltd. Zirconium oxychloride octahydrate ($ZrOCl_2{\cdot}8H_2O$), triethylene glycol dimethacrylate (TEGDMA), bisphenol A glycerolate dimethacrylate (Bis-GMA), zinc acetylacetonate, oleic acid, phenylcarbinol, camphorquinone (CQ), and ethyl-4-dimethylaminobenzoate (4-EDMAB) were bought from Shanghai Aladdin Biochemical Technology Co., Ltd. 3-Methacryloxypropyl trimethoxysilane (γ-MPS) was purchased from Alfa Aesar (China) Chemical Co., Ltd.

2.2. Preparation of inorganic nanodispersions

The SiO_2 nanodispersion was obtained according to the Stöber method [49]. First, deionized water (70 mL), $NH_3{\cdot}H_2O$ (6.4 mL), and ethanol (190 mL) were mixed and stirred at 60 °C in a 1000 mL flask. Then, a mixture containing TEOS (30 mL) and ethanol (190 mL) was poured into the above flask. The reaction lasted for 3 h at 60 °C.

The ZrO_2 nanodispersion was prepared based on a published work [50]. In brief, 10.473 g of $ZrOCl_2{\cdot}8H_2O$ was dissolved in 325 mL of deionized water at room temperature. A total of 190 mL of NaOH aqueous solution (0.125 mol·L^{-1}) was added dropwise into the above $ZrOCl_2$ solution under vigorous stirring. The mixture was then stirred at 70 °C for 3 h, followed by a dialysis process to thoroughly wash the as-obtained zirconium hydroxide precursor. Finally, the precursor was heat-treated at 170 °C for 10 h in a 1 L Teflon-lined stainless-steel autoclave to form the ZrO_2 nanodispersion.

The preparation of the ZnO nanodispersion was based on our previous work [43]. First, 5.272 g of zinc acetylacetonate, 2.4 mL of oleic acid, and 120 mL of phenylcarbinol were mixed and stirred at 60 °C for 3 h. The mixture was then heat-treated at 150 °C for 10 h in a 200 mL Teflon-lined stainless-steel autoclave. The obtained suspension was centrifuged and washed with ethyl alcohol for three times, followed by an ultrasonic treatment (Scientz-IID, Ningbo Scientz Biotechnology Co., Ltd., China) to obtain the ZnO nanodispersion.

2.3. Construction of CNCs using a spray dryer with a three-fluid nozzle

The SiO_2–ZrO_2 CNCs were constructed using a spray dryer with a three-fluid nozzle. SiO_2 and ZrO_2 nanodispersions with a solid content of 2% in mass fraction were simultaneously pumped into the spray dryer through two different liquid channels in the three-fluid nozzle. The aspirator level, inlet temperature, compressed air flow rate, and total feed rate were set at 100%, 100 °C, 600 L·h^{-1}, and 0.4 L·h^{-1}, respectively. For comparison, SiO_2–ZrO_2 CNCs and SNCs were also constructed by means of a two-fluid nozzle under the same spray drying conditions.

In order to prepare the SiO_2–ZrO_2–ZnO CNCs, first, the SiO_2 and ZnO nanodispersions (2% in mass fraction) were mixed to obtain a SiO_2–ZnO dispersion. Then, the above dispersion and the ZrO_2 nanodispersion (2% in mass fraction) were respectively pumped into the spray dryer through the three-fluid nozzle. The aspirator level, inlet

temperature, compressed air flow rate, and total feed rate were set at 100%, 100 °C, 600 L·h^{-1}, and 0.4 L·h^{-1}, respectively. Other CNCs including SiO_2–ZnO–CaF_2 CNCs, SiO_2–TiO_2–CaF_2 CNCs, SiO_2–ZnO–ZrO_2–TiO_2 CNCs, and SiO_2–ZnO–TiO_2–CaF_2 CNCs were constructed using the same three-fluid nozzle spray drying process as described above; the distributions of the raw materials in the two channels of the three-fluid nozzle are shown in Table S1 in Appendix A.

To confirm the influence of heat treatment on the filling properties of the SiO_2–ZrO_2 and SiO_2–ZrO_2–ZnO CNCs, the CNCs were calcined in a muffle furnace (LH 30/13, Nabertherm, China) at 500 °C for 3 h. All the inorganic fillers were coded, as shown in Table 1.

2.4. Preparation of DRCs

All the fillers were further silanized before being blended with the resin matrices (Bis-GMA and TEGDMA at a mass ratio of 1:1) and photoinitiators (CQ and 4-EDMAB at a mass ratio of 1:4, 1% in mass fraction of the matrices). The silanization process was done according to our previous work [41]. All the components were premixed by hand and then thoroughly blended using a three-roll mixer (TR50M, Trilos Precision Equipment Co., Ltd., China). The filler content was fixed at 70% in mass fraction. The well-mixed pastes were filled into different silicone rubber molds with various shapes and photopolymerized by means of light-emitting diode (LED) light curing (SLC-VIII B, 430–490 nm, Hangzhou Sifang Medical Apparatus Co., Ltd., China) for 120 s. All specimens were polished with silicon carbide papers before testing.

2.5. Characterization of CNCs

A transmission electron microscope (TEM; JEOL-7800, JEOL, Japan) was used to observe the nanoparticles at an accelerating voltage of 120 kV. The surface potentials of the nanoparticles were measured using a particle size and zeta potential analyzer (Nano ZS90, Malvern, UK). The morphology and size of the CNCs could be clearly seen via scanning electron microscopy (SEM; JSM-6701F, JEOL) with a 5 kV operating voltage. The crystal structures of the CNCs were confirmed by means of an X-ray diffractometer (D8 Advance, Bruker Optik GmbH, Germany). The distribution of the silicon (Si), zirconium (Zr), zinc (Zn), and oxygen (O) elements in the CNCs were observed using scanning electron microscopy-energy dispersive X-ray spectrometry (SEM-EDS) at 20 kV.

2.6. Characterization of resin composites

2.6.1. Mechanical properties

According to International Organization for Standardization (ISO) 4049:2009, the flexural strength and modulus of the DRCs were determined by means of a three-point bending test using a universal testing machine (CMT6503, MTS Industrial Systems Co., Ltd., China). Six specimens (25 mm × 2 mm × 2 mm) were bent in the machine with a span of 20 mm and crosshead speed of 0.75 mm·min^{-1}, respectively. Compressive strength was also tested by the universal testing machine using cylindrical specimens (ϕ4 mm × 6 mm, n = 6) with 0.75 mm·min^{-1} crosshead speed. Vickers microhardness was tested on the cylindrical samples (ϕ6 mm × 4 mm, n = 6) using a microhardness tester (HXD-1000TMC/LCD, Shanghai Taiming Optical Instrument Co., Ltd., China) under a 50 g load for 10 s.

2.6.2. Degree of conversion

A Fourier-transform infrared (FTIR) spectrometer equipped with an attenuated total reflectance crystal accessory (Vertex 70v, Bruker Optik GmbH) was used to analyze the degree of conversion of the DRCs. The spectra of cured and uncured DRCs were recorded in the range of 1700–1550 cm^{-1} with a resolution of 4 cm^{-1}. The conversion degree data were calculated based on the Eq. (1), where A_{1637} and A_{1608} represent the peak absorption of aliphatic C=C (1637 cm^{-1}) and aromatic C=C (1608 cm^{-1}), respectively.

$$\text{Degree of conversion} = \left[1 - \frac{(A_{1637}/A_{1608})_{\text{polymer}}}{(A_{1637}/A_{1608})_{\text{monomer}}}\right] \times 100\% \quad (1)$$

2.6.3. Radiopacity

Disc-shaped samples (ϕ10 mm × 1 mm) were prepared for each type of DRC and were irradiated with X-rays (70 kV, 8 mA, 0.1 s), along with a standard aluminum (Al) step-wedge having 12 steps ranging from 0.5 to 6 mm, to obtain radiographs. The optical density of each material in the radiographs was measured using an optical density meter (LS117, Shenzhen Linshang Technology Co. Ltd., China). The radiopacity of the samples was expressed in terms of equivalent Al thickness (mm).

2.6.4. Antibacterial activity

The antibacterial activity of the DRCs was determined through a quantitative analysis based on American Society for Testing and Materials (ASTM) E2180–07(2012). Inoculated molten agar slurry (0.08 mL) containing approximately 10^6 colony-forming units (CFU) of *Streptococcus mutans* (*S. mutans*) was pipetted onto the DRCs (ϕ20 mm × 2 mm, n = 3) and was then incubated at 37 °C for 24 h. The surviving *S. mutans* after incubation was obtained by the elution of the agar slurry inoculum with Dey/Engley (D/E) neutralizing broth. The serial dilutions were spread on tryptic soy agar, and then incubated for 48 h. Finally, the bacterial colonies were counted and recorded. The *S. mutans* incubated without DRCs was adopted as a blank sample. The antibacterial ratio of the DRCs was calculated by Eq. (2).

$$\text{Antibacterial ratio} = \frac{a-b}{a} \times 100\% \quad (2)$$

where a represents the antilog of the geometric mean of the number of bacteria recovered from the incubation period in the blank samples, and b represents the antilog of the geometric mean of

Table 1
Codes of different inorganic fillers.

Code	Inorganic filler (% in mass fraction)			Heat treatment	Nozzle type
	SiO_2	ZrO_2	ZnO		
SNCs	70	0	0	No	Two-fluid nozzle
$Si_{60}Zr_{10}$-2	60	10	0	No	Two-fluid nozzle
$Si_{60}Zr_{10}$-3	60	10	0	No	Three-fluid nozzle
H-$Si_{64}Zr_6$-3	64	6	0	Yes	Three-fluid nozzle
H-$Si_{62}Zr_8$-3	62	8	0	Yes	Three-fluid nozzle
H-$Si_{60}Zr_{10}$-3	60	10	0	Yes	Three-fluid nozzle
H-$Si_{58}Zr_{12}$-3	58	12	0	Yes	Three-fluid nozzle
H-$Si_{56}Zr_{10}Zn_4$-3	56	10	4	Yes	Three-fluid nozzle

the number of bacteria recovered from the incubation period in the experimental samples.

2.7. Statistical analysis

The statistical significance was evaluated with SPSS software using one-way analysis of variance (ANOVA) with Tukey's test with a 95% confidence interval.

3. Results and discussion

Fig. 1 shows a schematic diagram for the preparation process of SiO_2–ZrO_2 CNCs by means of a spray dryer with a two-fluid nozzle and a three-fluid nozzle, respectively. The raw materials (SiO_2 and ZrO_2 nanodispersions) for the spray drying process were transparent, and the nanoparticles were well dispersed in the mediums (Figs. 1(a) and (b)). A two-fluid nozzle has only one liquid channel and one gas channel (Fig. 1(d)), whereas a three-fluid nozzle includes two liquid channels (Fig. 1(g)). Therefore, the SiO_2 and ZrO_2 nanodispersions had to be mixed before being pumped into the spray dryer through the two-fluid nozzle. However, the zeta potentials of the SiO_2 (−31 mV) and ZrO_2 (+47 mV) nanoparticles are opposite. This resulted in severe aggregation of nanoparticles, the formation of an opaque nanodispersion, and even precipitation after both nanodispersions were mixed (Fig. 1(c)). As a result, the SiO_2–ZrO_2 CNCs fabricated by the two-fluid nozzle appeared to have an irregular shape (Fig. 1(e)).

The use of a three-fluid nozzle can avoid unwanted aggregation before the spray drying process by separating nanodispersions with opposite zeta potentials; in this case, the SiO_2 and ZrO_2 nanodispersions were simultaneously and respectively pumped into the spray dryer through different channels of the three-fluid nozzle (Fig. 1(f)). The nanodispersions were instantaneously mixed and immediately atomized into microdroplets by compressed air at the end of the nozzle. Meanwhile, the solvent was evaporated from the droplet surface by a gas stream at 100 °C. The SiO_2–ZrO_2 CNCs were thus constructed when the solvent was completely evaporated. Fig. 1(h) displays an SEM image of $Si_{60}Zr_{10}$-3. The regular shape and closely packed structure (similar to those of the SNCs [41]) demonstrate that the incorporation of ZrO_2 nanoparticles did not affect the morphology of the NCs.

The mechanical properties of the DRCs filled with SNCs, $Si_{60}Zr_{10}$-2, and $Si_{60}Zr_{10}$-3 are shown in Fig. 2. Compared with the performances of the SNCs-filled DRCs, the flexural strength and compressive strength of the $Si_{60}Zr_{10}$-2-filled DRCs showed a significant decrease (of 16% and 17%, respectively), which was probably due to the irregular and relatively loose structure of $Si_{60}Zr_{10}$-2. In contrast, the $Si_{60}Zr_{10}$-3-filled DRCs exhibited good mechanical properties comparable to those of the SNC-filled DRCs, thus demonstrating that the structure of the CNCs is important for their filling properties, and that the three-fluid nozzle is suitable for spray drying components that are incompatible due to opposite zeta potentials.

CNCs with different SiO_2–ZrO_2 ratios were further constructed by means of the three-fluid nozzle, and were then heat-treated at 500 °C for 3 h to improve their filling properties (labeled as H-$Si_{64}Zr_6$-3, H-$Si_{62}Zr_8$-3, H-$Si_{60}Zr_{10}$-3, and H-$Si_{58}Zr_{12}$-3), since our previous work [51] demonstrated that the heat treatment process can strengthen the CNC structure. The morphologies of the SiO_2–ZrO_2 CNCs are shown in Fig. 3, and the corresponding size distributions are displayed in Fig. S1 in Appendix A. All the CNCs exhibited a regular shape and closely packed structure. Their average sizes increased from 1.20 to 1.89 μm as the ZrO_2 content was increased from 6/70 to 12/70.

Fig. 4 shows the X-ray diffraction (XRD) patterns of CNCs with different SiO_2–ZrO_2 ratios. The broad diffraction peak at 23° indicates that the SiO_2 nanoparticles are amorphous, which is specified in Powder Diffraction File (PDF) card No. 29–0085. The diffraction peaks at 28.34°, 31.48°, 40.89°, and 45.51° belong to monoclinic-phase ZrO_2, according to PDF card No. 80–0966, and the peaks at 30°, 35°, 50.37°, and 60.19° can be ascribed to tetragonal-phase ZrO_2 (PDF card No. 88–1007). These findings indicate that the ZrO_2 nanocrystals are a mixture of tetragonal and monoclinic phases [50]. In addition, the peaks of ZrO_2 became stronger with the increase of ZrO_2 content. To confirm the distributions of SiO_2 and ZrO_2 in the CNCs, the O, Si, and Zr elements in H-$Si_{60}Zr_{10}$-3

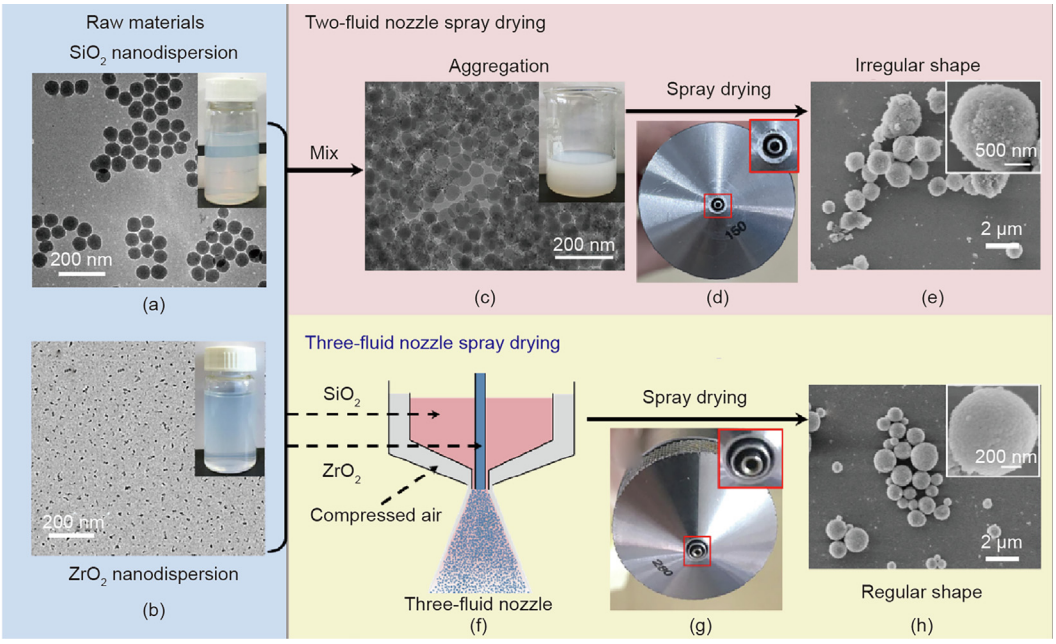

Fig. 1. Schematic diagrams for the preparation process of SiO_2–ZrO_2 CNCs using a spray dryer equipped with a two-fluid nozzle or a three-fluid nozzle. (a) TEM image and photograph of the SiO_2 nanodispersion; (b) TEM image and photograph of the ZrO_2 nanodispersion; (c) TEM image and photograph of the SiO_2 and ZrO_2 mixture; (d) photograph of the two-fluid nozzle; (e) SEM images of $Si_{60}Zr_{10}$-2; (f) scheme of SiO_2 and ZrO_2 nanodispersions in the three-fluid nozzle; (g) photograph of the three-fluid nozzle; (h) SEM images of $Si_{60}Zr_{10}$-3.

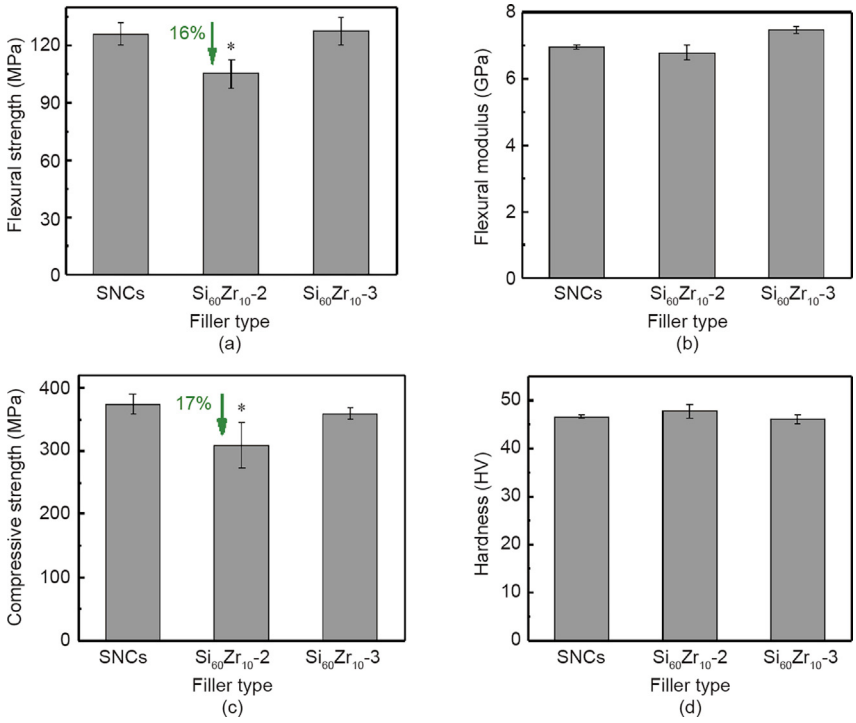

Fig. 2. (a) Flexural strength, (b) flexural modulus, (c) compressive strength, and (d) hardness of DRCs filled with SNCs, $Si_{60}Zr_{10}$-2, and $Si_{60}Zr_{10}$-3, respectively. *: $p < 0.05$ compared with the DRCs filled with SNCs.

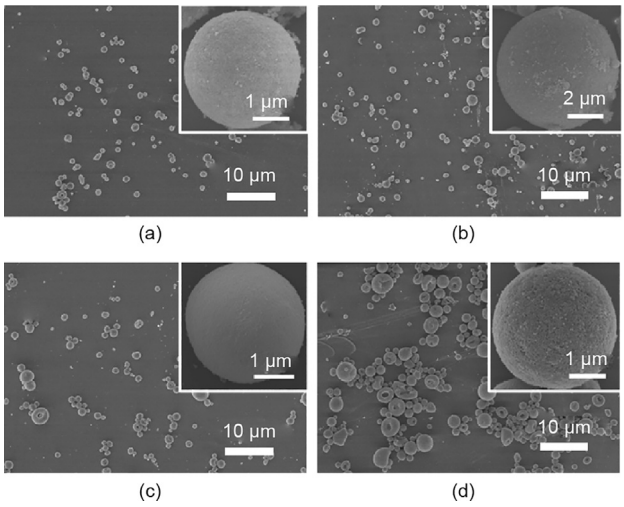

Fig. 3. SEM images of (a) H-$Si_{64}Zr_6$-3, (b) H-$Si_{62}Zr_8$-3, (c) H-$Si_{60}Zr_{10}$-3, and (d) H-$Si_{58}Zr_{12}$-3.

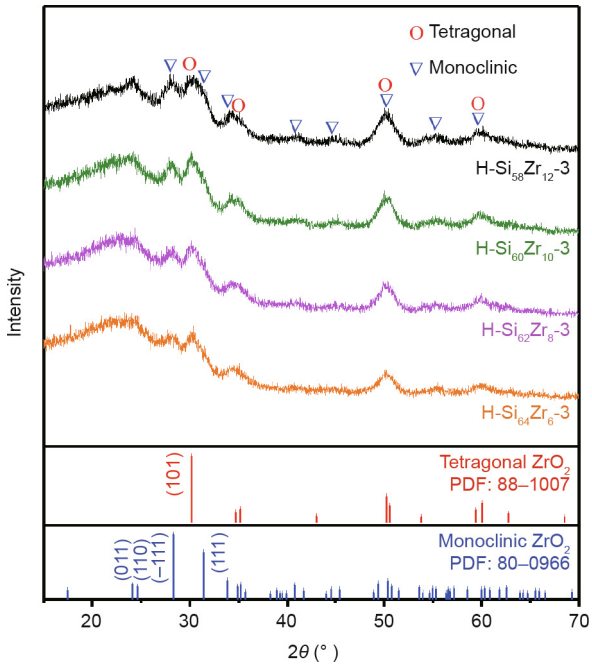

Fig. 4. X-ray diffraction (XRD) patterns of H-$Si_{64}Zr_6$-3, H-$Si_{62}Zr_8$-3, H-$Si_{60}Zr_{10}$-3, and H-$Si_{58}Zr_{12}$-3.

were directly observed using SEM-EDS maps (Fig. 5). Fig. 5(a) clearly shows that all the elements are evenly distributed in H-$Si_{60}Zr_{10}$-3, as is also evidenced by the even and spherical distribution of the Si and Zr elements in Fig. 5(b). These results demonstrate that the CNCs are successfully composed of ZrO_2 and SiO_2 nanoparticles with even distributions.

Fig. 6 shows the mechanical properties of the DRCs containing heat-treated CNCs (H-$Si_{60}Zr_{10}$-3) and untreated CNCs ($Si_{60}Zr_{10}$-3). The heat treatment process clearly and dramatically enhanced the filling properties of the CNCs, especially in terms of the flexural modulus and hardness of the DRCs, which increased by 18% and 40% compared with those of the DRCs filled with untreated CNCs. The main reason for this increase is that the heat treatment process enhanced the interaction among the nanoparticles, resulting in a more compact structure and a densified framework in the CNCs [46], as evidenced by the fracture surfaces of the DRCs (Fig. 7). The $Si_{60}Zr_{10}$-3-filled DRCs exhibited a flat surface (Fig. 7(a)), indicating weak resistance to an externally applied force. The CNC structure cannot be clearly seen in Fig. 7(a); this demonstrates that the nanoparticles in the untreated CNCs are unstable, which may

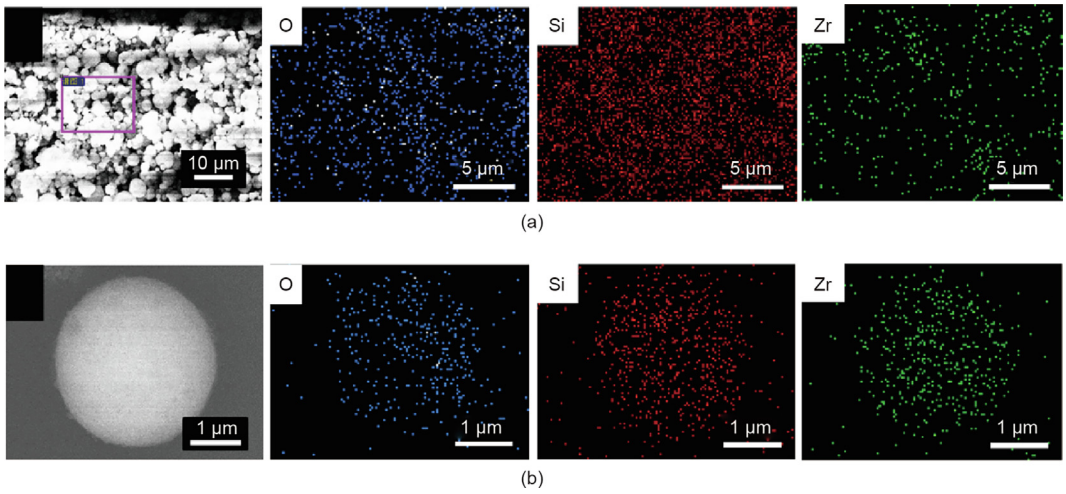

Fig. 5. SEM-EDS maps for O, Si, and Zr in H-$Si_{60}Zr_{10}$-3. (a) Holistic element distributions; (b) element distributions in a single CNC.

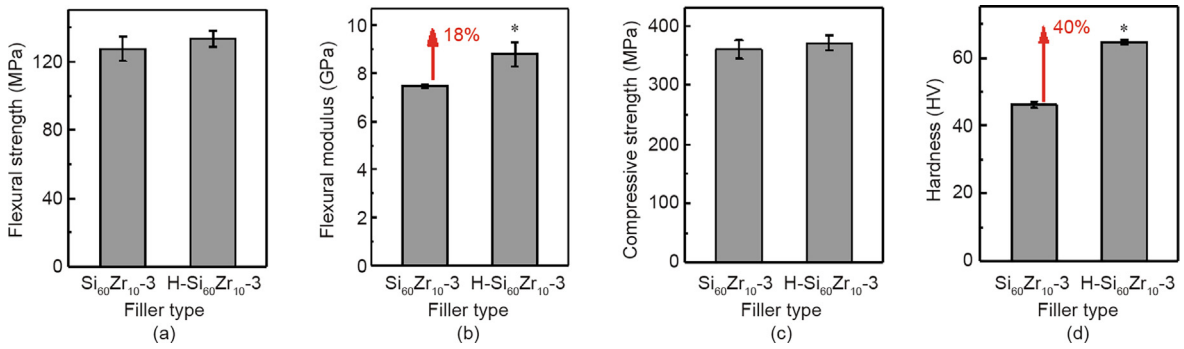

Fig. 6. (a) Flexural strength, (b) flexural modulus, (c) compressive strength, and (d) hardness of the DRCs filled with $Si_{60}Zr_{10}$-3 and H-$Si_{60}Zr_{10}$-3. *: $p < 0.05$ compared with the DRCs filled with $Si_{60}Zr_{10}$-3.

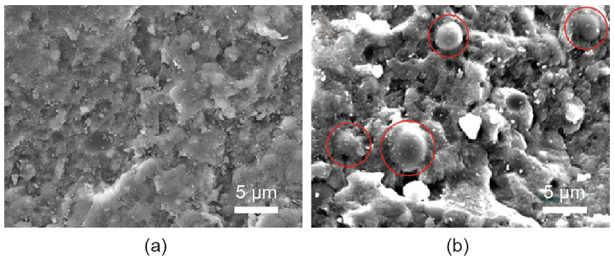

Fig. 7. SEM images of the fracture surfaces of DRCs filled with (a) $Si_{60}Zr_{10}$-3 and (b) H-$Si_{60}Zr_{10}$-3.

result in destruction after they are extruded from the three-roll extruder. After the heat treatment process, the H-$Si_{60}Zr_{10}$-3 exhibited a stronger structure, since many complete H-$Si_{60}Zr_{10}$-3 can be seen on the cross-section of the DRCs (red circles in Fig. 7(b)). The DRCs displayed a coarse fracture surface with several curved steps, demonstrating the crack deflection caused by the addition of H-$Si_{60}Zr_{10}$-3 and the higher fracture energy of the DRCs [42]. The conversion degrees showed no significant difference between the heat-treated and untreated CNC-filled DRCs (Fig. S2 in Appendix A).

Fig. 8 gives the radiographs and radiopacity of DRCs filled with different types of fillers; the corresponding data are listed in Appendix A Table S2. Fig. 8(a) shows the radiograph of the Al steps and the DRCs filled with SNCs, $Si_{60}Zr_{10}$-3, and H-$Si_{60}Zr_{10}$-3. The optical densities of the Al steps in the radiograph show a linear decline (Fig. 8(c)) with the increased thicknesses, indicating the enhanced radiopacity. The SNC-filled DRC displays the lowest radiopacity, which is only equivalent to a 0.14 mm Al step (Table S2), while the DRCs filled with $Si_{60}Zr_{10}$-3 and H-$Si_{60}Zr_{10}$-3 are equivalent to the 0.57 and 1.02 mm Al steps, respectively. These results indicate that the addition of ZrO_2 nanoparticles significantly improves the radiopacity of the DRCs, and that the heat treatment process for the fillers can further strengthen this property.

DRCs loaded with H-$Si_{64}Zr_6$-3, H-$Si_{62}Zr_8$-3, H-$Si_{60}Zr_{10}$-3, and H-$Si_{58}Zr_{12}$-3 were prepared in order to explore the influence of ZrO_2 content on the radiopacity (Fig. 8(b)). It became evident that an increase of ZrO_2 content from 6% to 12% in mass fraction led to a significant increment from 0.36 to 1.3 mm of the radiopacity of the DRCs (Table S2). According to ISO 4049:2009, the radiopacity of DRCs must be equal to or higher than that of the same thickness of Al, which means that the H-$Si_{60}Zr_{10}$-3-filled DRCs and H-$Si_{58}Zr_{12}$-3-filled DRCs can meet this standard.

S. mutans is commonly regarded as the primary pathogenic bacteria of dental caries [52,53]. Plaque accumulating at the margin of DRCs may result in secondary caries, and may shorten the service life of the DRCs [54,55]. Therefore, ZnO nanoparticles (Fig. S3 in Appendix A) were introduced into the CNCs by means of a three-fluid nozzle spray drying process in order to provide the DRCs with antibacterial activity. Fig. 9 shows SEM images of H-$Si_{56}Zr_{10}Zn_4$-3, along with the corresponding XRD pattern and SEM-EDS maps. H-$Si_{56}Zr_{10}Zn_4$-3 maintains a regular shape (Fig. 9(a)), and all the components are successfully imbedded into the CNCs (Fig. 9(b)).

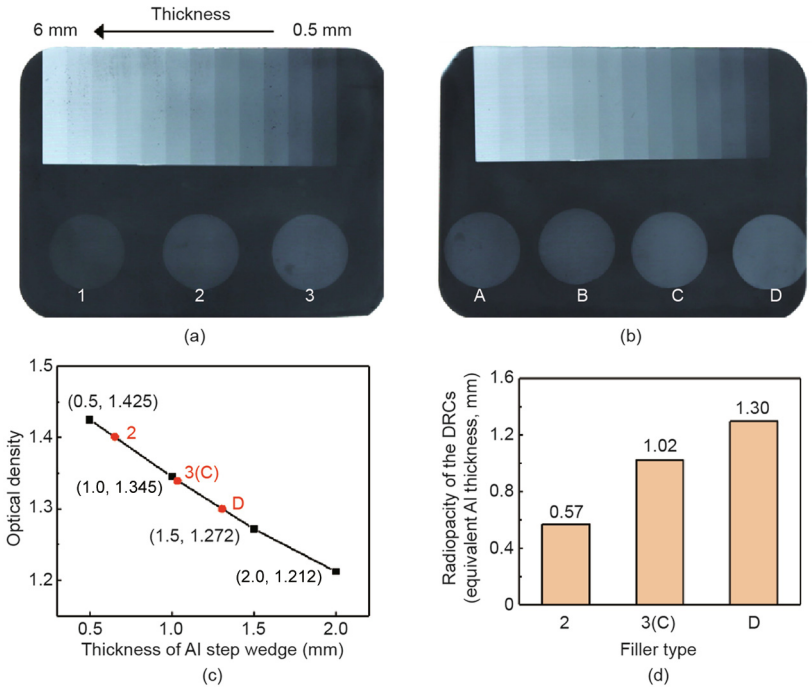

Fig. 8. (a, b) Radiographs and (c, d) radiopacity data of DRCs filled with different types of fillers. 1: SNCs; 2: $Si_{60}Zr_{10}$-3; 3: H-$Si_{60}Zr_{10}$-3. A: H-$Si_{64}Zr_6$-3; B: H-$Si_{62}Zr_8$-3; C: H-$Si_{60}Zr_{10}$-3; D: H-$Si_{58}Zr_{12}$-3. The aluminum steps were used as a reference.

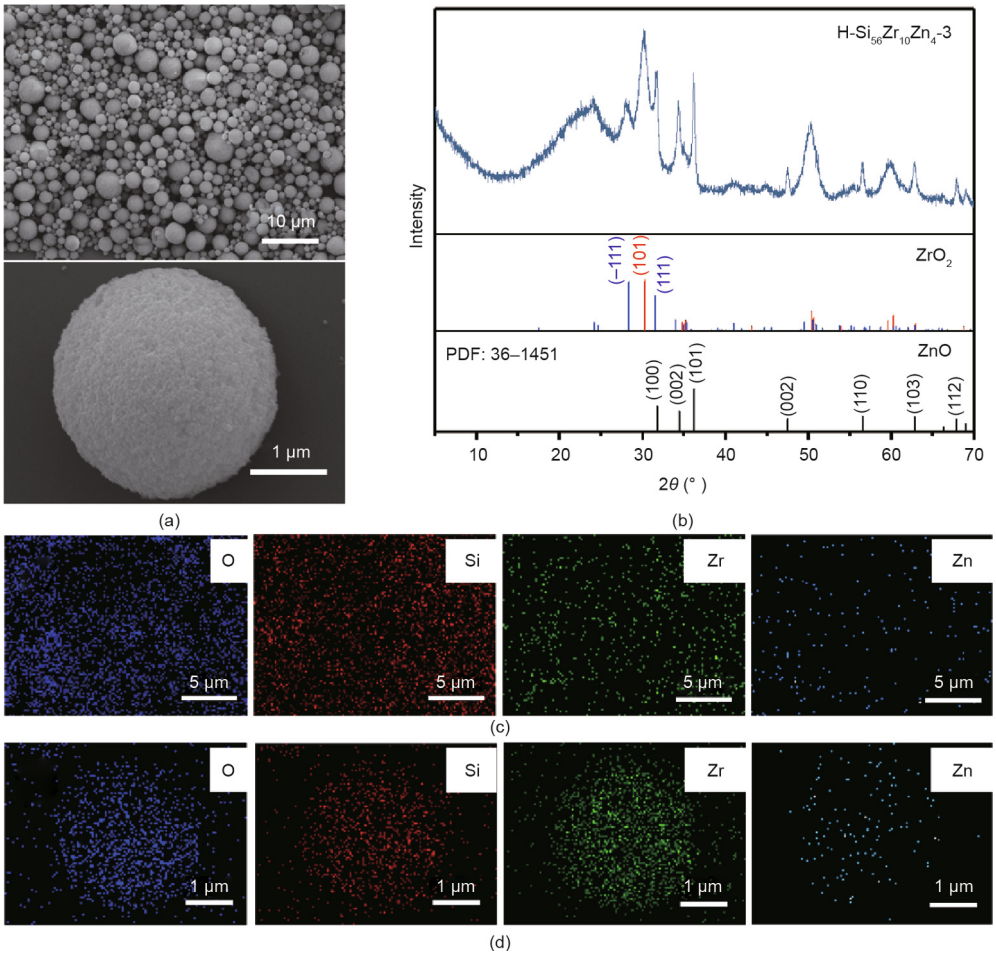

Fig. 9. (a) SEM images and (b) XRD pattern of H-$Si_{56}Zr_{10}Zn_4$-3; (c, d) SEM-EDS maps for O, Si, Zr, and Zn elements in H-$Si_{56}Zr_{10}Zn_4$-3.

The element distributions of O, Si, Zr, and Zn are even (Figs. 9(c) and (d)), which is due to the good dispersion of the raw materials pumped into the spray dryer.

Fig. 10 shows the properties of the H-$Si_{60}Zr_{10}$-3-filled and H-$Si_{56}Zr_{10}Zn_4$-3-filled DRCs. The flexural properties, compressive strength, and degree of conversion of the H-$Si_{56}Zr_{10}Zn_4$-3-filled DRCs show no significant difference in comparison with those of the H-$Si_{60}Zr_{10}$-3-filled DRCs, which demonstrates that the introduction of the ZnO nanoparticles did not destroy the advantageous structure of the CNCs. However, the hardness decreases from (64.5 ± 0.7) to (61.7 ± 0.2) HV. This decrease is mainly because the ZnO nanoparticles are not as hard as the SiO_2 and ZrO_2 nanoparticles. In addition, the radiopacity of the DRCs slightly increases from 1.02 to 1.08 mm (in terms of equivalent Al thickness).

To quantitatively analyze the antibacterial activity of the H-$Si_{56}Zr_{10}Zn_4$-3-filled DRCs, *S. mutans* was adopted in this study. Fig. 11 shows photographs of surviving *S. mutans* after being incubated for different times in the blank and experimental groups. For the blank group, the number of live *S. mutans* significantly increased after being incubated for 24 h (Figs. 11(a) and (b)). The number of *S. mutans* cultured on the H-$Si_{60}Zr_{10}$-3-filled DRCs for 24 h showed no significant difference in comparison with those cultured on the blank group, indicating that the composites loaded with the SiO_2–ZrO_2 CNCs have no antibacterial activity. In contrast, the growth of the *S. mutans* incubated on the H-$Si_{56}Zr_{10}Zn_4$-3-filled DRCs was obviously inhibited (Fig. 11(d)), and the antibacterial ratio exceeded 99.9%. These results demonstrate that H-$Si_{56}Zr_{10}Zn_4$-3 has great potential as an antibacterial filler.

To confirm the universality of three-fluid nozzle spray drying, TiO_2 (Fig. S4(a) in Appendix A) and CaF_2 (Fig. S4(b) in Appendix A) nanoparticles—which are also commonly used dental fillers—were adopted as co-fillers of SiO_2 nanoparticles to construct CNCs. The zeta potentials of CaF_2 and TiO_2 nanoparticles are +55.6 and +45.2 mV, which are opposite with that of SiO_2 nanoparticles. Therefore, it is appropriate to use three-fluid nozzle spray drying. Various CNCs were constructed using three or four kinds of nanoparticles as building blocks, including SiO_2–ZnO–CaF_2 CNCs (Fig. 12(a)), SiO_2–TiO_2–CaF_2 CNCs (Fig. 12(b)), SiO_2–ZnO–ZrO_2–TiO_2 CNCs (Fig. 12(c)), and SiO_2–ZnO–TiO_2–CaF_2 CNCs (Fig. 12(d)). The mass ratios of the different nanoparticles are shown in Table S1. All the CNCs exhibited a regular shape, thereby demonstrating that three-fluid nozzle spray drying is a feasible and general strategy for constructing multifunctional fillers for DRCs.

4. Conclusions

In this study, multifunctional CNCs were successfully constructed using a spray dryer with a three-fluid nozzle for DRCs. The use of the three-fluid nozzle effectively avoided the unwanted aggregation of different nanoparticles with opposite zeta potentials before the spray drying process, thus achieving regular-shaped CNCs with evenly distributed elements. For the SiO_2–ZrO_2 binary system, the mechanical properties of the $Si_{60}Zr_{10}$-3-filled DRCs were consistent with those of SNC-filled DRCs because the regular CNC structure was maintained. The CNCs were also heat treated to reinforce their structure, thus obtaining better filling properties. Compared with the DRCs filled with untreated CNCs, the heat-treated CNC-filled DRCs exhibited significantly improved mechanical properties, particularly in terms of the flexural modulus (an increase of 18%) and hardness (an increase of 40%). In addition, increasing the ZrO_2 content and using the heat treatment process for the CNCs resulted in DRCs with significantly enhanced radiopacity. The heat-treated CNC-filled DRCs containing over 10% (in mass fraction) ZrO_2 nanoparticles meet the requirement for radiopaque fillers. For the SiO_2–ZrO_2–ZnO ternary system, the antibacterial ratio of the H-$Si_{56}Zr_{10}Zn_4$-3-filled DRCs reached 99.9% while the mechanical properties remained stable. This

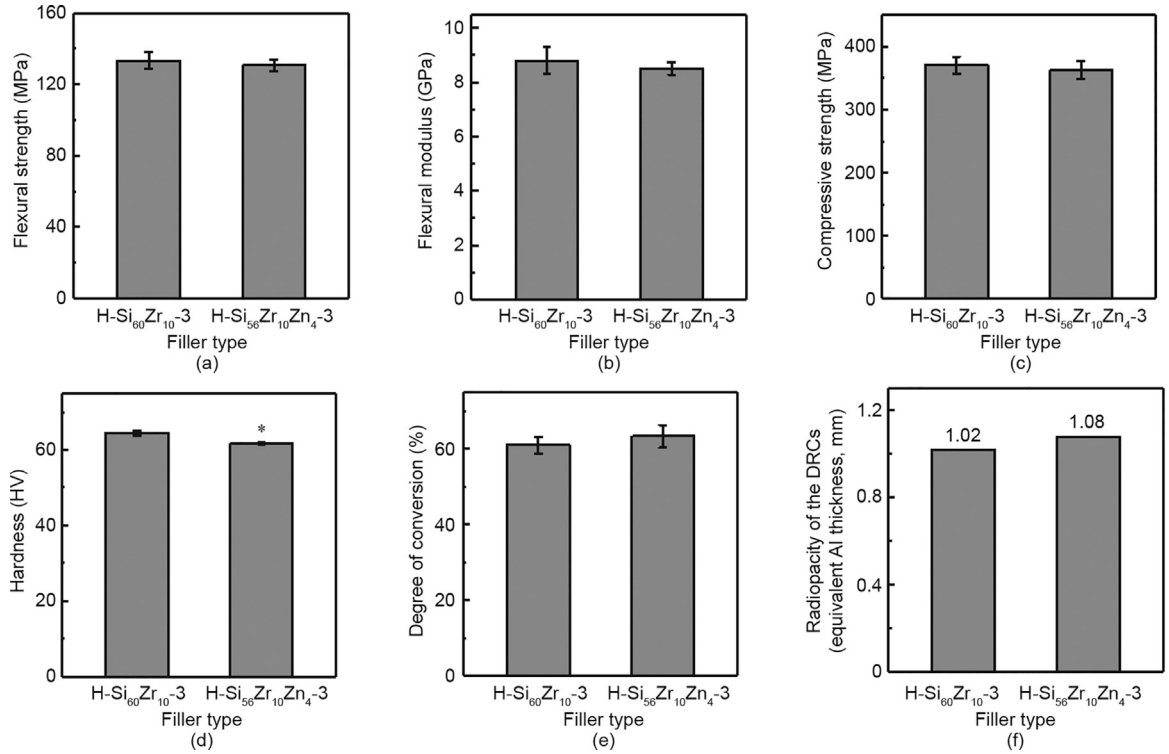

Fig. 10. (a) Flexural strength, (b) flexural modulus, (c) compressive strength, (d) hardness, (e) degree of conversion, and (f) radiopacity of H-$Si_{60}Zr_{10}$-3-filled and H-$Si_{56}Zr_{10}Zn_4$-3-filled DRCs. *: $p < 0.05$ compared with the DRCs filled with H-$Si_{60}Zr_{10}$-3.

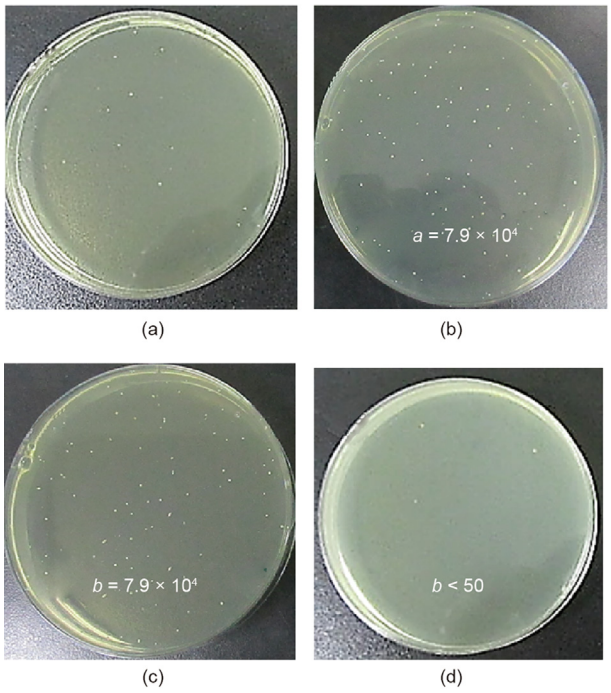

Fig. 11. Photographs of surviving *S. mutans* after being incubated for different times. (a) 0 h, blank group; (b) 24 h, blank group; (c) 24 h, H-$Si_{60}Zr_{10}$-3-filled DRCs; (d) 24 h, H-$Si_{56}Zr_{10}Zn_4$-3-filled DRCs.

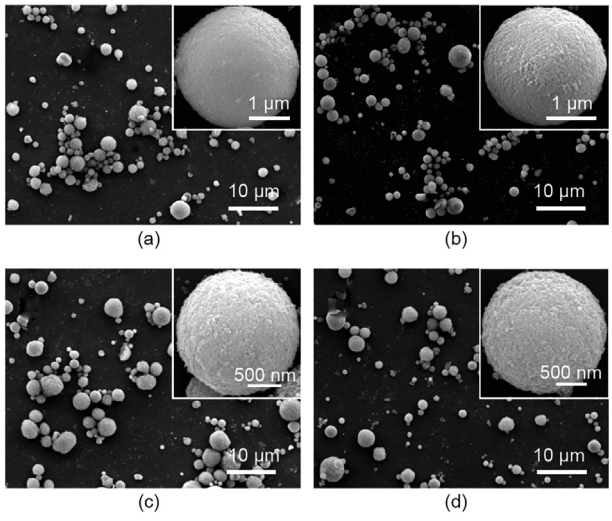

Fig. 12. SEM images of (a) SiO_2–ZnO–CaF_2 CNCs, (b) SiO_2–TiO_2–CaF_2 CNCs, (c) SiO_2–ZnO–ZrO_2–TiO_2 CNCs, and (d) SiO_2–ZnO–TiO_2–CaF_2 CNCs constructed by means of the three-fluid nozzle spray drying technique.

method can also be extended to other ternary and even quaternary systems. Therefore, this work provides a general strategy to construct high-performance multifunctional cluster fillers for DRCs, especially when simultaneously considering the mechanical performance, radiopacity, and antibacterial activity.

Acknowledgments

This work was financially supported by the National Key Research and Development Program of China (2016YFA0201701) and the National Natural Science Foundation of China (21878015).

Compliance with ethics guidelines

Dan-Lei Yang, Dan Wang, Hao Niu, Rui-Li Wang, Mei Liu, Fei-Min Zhang, Jie-Xin Wang, and Mei-Fang Zhu declare that they have no conflict of interest or financial conflicts to disclose.

Appendix A. Supplementary data

Supplementary data to this article can be found online at https://doi.org/10.1016/j.eng.2021.08.001.

References

[1] Li P, Zhang X, Hou C, Chen Y, He T. Highly efficient visible-light driven solar-fuel production over tetra(4-carboxyphenyl) porphyrin iron(III) chloride using CdS/Bi_2S_3 heterostructure as photosensitizer. Appl Catal B 2018;238:656–63.
[2] Wang Z, Zhao Z, Baucom J, Wang D, Dai L, Chen JF. Nitrogen-doped graphene foam as a metal-free catalyst for reduction reactions under a high gravity field. Engineering 2020;6(6):680–7.
[3] Liu L, Han J, Xu L, Zhou J, Zhao C, Ding S, et al. Aligned, high-density semiconducting carbon nanotube arrays for high-performance electronics. Science 2020;368(6493):850–6.
[4] Schrauben JN, Hayoun R, Valdez CN, Braten M, Fridley L, Mayer JM. Titanium and zinc oxide nanoparticles are proton-coupled electron transfer agents. Science 2012;336(6086):1298–301.
[5] Draz MS, Vasan A, Muthupandian A, Kanakasabapathy MK, Thirumalaraju P, Sreeram A, et al. Virus detection using nanoparticles and deep neural network-enabled smartphone system. Sci Adv 2020;6(51):eabd5354.
[6] Wang D, Wang Z, Zhan Q, Pu Y, Wang JX, Foster NR, et al. Facile and scalable preparation of fluorescent carbon dots for multifunctional applications. Engineering 2017;3(3):402–8.
[7] Casamonti M, Risaliti L, Vanti G, Piazzini V, Bergonzi MC, Bilia AR. Andrographolide loaded in micro- and nano-formulations: improved bioavailability, target-tissue distribution, and efficacy of the "king of bitters." Engineering 2019;5(1):69–75.
[8] McGillicuddy E, Morrison L, Cormican M, Dockery P, Morris D. Activated charcoal as a capture material for silver nanoparticles in environmental water samples. Sci Total Environ 2018;645:356–62.
[9] Chun K, Choi H, Lee J. Comparison of mechanical property and role between enamel and dentin in the human teeth. J Dent Biomech 2014;5:1758736014520809.
[10] Selwitz RH, Ismail AI, Pitts NB. Dental caries. Lancet 2007;369(9555):51–9.
[11] Aydin Sevinç B, Hanley L. Antibacterial activity of dental composites containing zinc oxide nanoparticles. J Biomed Mater Res B Appl Biomater 2010;94(1):22–31.
[12] Sideridou I, Tserki V, Papanastasiou G. Effect of chemical structure on degree of conversion in light-cured dimethacrylate-based dental resins. Biomaterials 2002;23(8):1819–29.
[13] Cramer NB, Stansbury JW, Bowman CN. Recent advances and developments in composite dental restorative materials. J Dent Res 2011;90(4):402–16.
[14] Par M, Spanovic N, Bjelovucic R, Skenderovic H, Gamulin O, Tarle Z. Curing potential of experimental resin composites with systematically varying amount of bioactive glass: degree of conversion, light transmittance and depth of cure. J Dent 2018;75:113–20.
[15] Besinis A, van Noort R, Martin N. Remineralization potential of fully demineralized dentin infiltrated with silica and hydroxyapatite nanoparticles. Dent Mater 2014;30(3):249–62.
[16] Makvandi P, Ghaemy M, Ghadiri AA, Mohseni M. Photocurable, antimicrobial quaternary ammonium-modified nanosilica. J Dent Res 2015;94(10):1401–7.
[17] Curtis AR, Shortall AC, Marquis PM, Palin WM. Water uptake and strength characteristics of a nanofilled resin-based composite. J Dent 2008;36(3):186–93.
[18] Leprince J, Palin WM, Mullier T, Devaux J, Vreven J, Leloup G. Investigating filler morphology and mechanical properties of new low-shrinkage resin composite types. J Oral Rehabil 2010;37(5):364–76.
[19] Niu H, Yang DL, Sun Q, Pu Y, Gao T, Wang JX. A new method for predicting the maximum filler loading of dental resin composites based on DEM simulations and experiments. Dent Mater 2020;36(12):e375–85.
[20] Qian L, Wang R, Li W, Chen H, Jiang X, Zhu M. The synthesis of urchin-like serried hydroxyapatite (USHA) and its reinforcing effect for dental resin composites. Macromol Mater Eng 2019;304(5):1800738
[21] Chadda H, Satapathy BK, Patnaik A, Ray AR. Mechanistic interpretations of fracture toughness and correlations to wear behavior of hydroxyapatite and silica/hydroxyapatite filled bis-GMA/TEGDMA micro/hybrid dental restorative composites. Compos Part B Eng 2017;130:132–46.
[22] Tammaro L, Di Salle A, Calarco A, De Luca I, Riccitiello F, Peluso G, et al. Multifunctional bioactive resin for dental restorative materials. Polymers 2020;12(2):332.
[23] Weir MD, Moreau JL, Levine ED, Strassler HE, Chow LC, Xu HHK. Nanocomposite containing CaF_2 nanoparticles: thermal cycling, wear and long-term water-aging. Dent Mater 2012;28(6):642–52.

[24] Pandit S, Kim GR, Lee MH, Jeon JG. Evaluation of *Streptococcus mutans* biofilms formed on fluoride releasing and non fluoride releasing resin composites. J Dent 2011;39(11):780–7.
[25] Yoshida K, Tanagawa M, Atsuta M. Characterization and inhibitory effect of antibacterial dental resin composites incorporating silver-supported materials. J Biomed Mater Res 1999;47(4):516–22.
[26] Tavassoli Hojati S, Alaghemand H, Hamze F, Ahmadian Babaki F, Rajab-Nia R, Rezvani MB, et al. Antibacterial, physical and mechanical properties of flowable resin composites containing zinc oxide nanoparticles. Dent Mater 2013;29(5):495–505.
[27] Taira M, Toyooka H, Miyawaki H, Yamaki M. Studies on the radiopacity of experimental dental composite resins containing admixed SiO_2–ZrO_2 fillers. J Mater Sci Mater M 1995;6(1):5–7.
[28] Bowen RL, Cleek GW. A new series of X-ray-opaque reinforcing fillers for composite materials. J Dent Res 1972;51(1):177–82.
[29] Chiari MDS, Rodrigues MC, Xavier TA, de Souza EMN, Arana-Chavez VE, Braga RR. Mechanical properties and ion release from bioactive restorative composites containing glass fillers and calcium phosphate nano-structured particles. Dent Mater 2015;31(6):726–33.
[30] Xu HH, Moreau JL, Sun L, Chow LC. Nanocomposite containing amorphous calcium phosphate nanoparticles for caries inhibition. Dent Mater 2011;27(8):762–9.
[31] Samuel SP, Li S, Mukherjee I, Guo Y, Patel AC, Baran G, et al. Mechanical properties of experimental dental composites containing a combination of mesoporous and nonporous spherical silica as fillers. Dent Mater 2009;25(3):296–301.
[32] Wang X, Cai Q, Zhang X, Wei Y, Xu M, Yang X, et al. Improved performance of Bis-GMA/TEGDMA dental composites by net-like structures formed from SiO_2 nanofiber fillers. Mater Sci Eng C 2016;59:464–70.
[33] Wang R, Zhang M, Liu F, Bao S, Wu T, Jiang X, et al. Investigation on the physical–mechanical properties of dental resin composites reinforced with novel bimodal silica nanostructures. Mater Sci Eng C 2015;50:266–73.
[34] Atai M, Pahlavan A, Moin N. Nano-porous thermally sintered nano silica as novel fillers for dental composites. Dent Mater 2012;28(2):133–45.
[35] Rodríguez HA, Giraldo LF, Casanova H. Formation of functionalized nanoclusters by solvent evaporation and their effect on the physicochemical properties of dental composite resins. Dent Mater 2015;31(7):789–98.
[36] Waldron K, Wu WD, Wu Z, Liu W, Selomulya C, Zhao D, et al. Formation of monodisperse mesoporous silica microparticles via spray-drying. J Colloid Interface Sci 2014;418:225–33.
[37] Dantas D, Pasquali MA, Cavalcanti-Mata M, Duarte ME, Lisboa HM. Influence of spray drying conditions on the properties of avocado powder drink. Food Chem 2018;266:284–91.
[38] Glavas L, Odelius K, Albertsson AC. Simultaneous polymerization and polypeptide particle production via reactive spray-drying. Biomacromolecules 2016;17(9):2930–6.
[39] Balgis R, Ernawati L, Ogi T, Okuyama K, Gradon L. Controlled surface topography of nanostructured particles prepared by spray-drying process. AIChE J 2017;63(5):1503–11.
[40] Iskandar F, Gradon L, Okuyama K. Control of the morphology of nanostructured particles prepared by the spray drying of a nanoparticle sol. J Colloid Interface Sci 2003;265(2):296–303.
[41] Yang DL, Sun Q, Duan YH, Niu H, Wang RL, Wang D, et al. Efficient construction of SiO_2 colloidal nanoparticle clusters as novel fillers by a spray-drying process for dental composites. Ind Eng Chem Res 2019;58(39):18178–86.
[42] Zhao SN, Yang DL, Wang D, Pu Y, Le Y, Wang JX, et al. Design and efficient fabrication of micro-sized clusters of hydroxyapatite nanorods for dental resin composites. J Mater Sci 2019;54(5):3878–92.
[43] Yang DL, Cui YN, Sun Q, Liu M, Niu H, Wang JX. Antibacterial activity and reinforcing effect of SiO_2–ZnO complex cluster fillers for dental resin composites. Biomater Sci 2021;9(5):1795–804.
[44] Kašpar O, Jakubec M, Štěpánek F. Characterization of spray dried chitosan-TPP microparticles formed by two- and three-fluid nozzles. Powder Technol 2013;240(5):31–40.
[45] Wang C, Hickey AJ. Isoxyl aerosols for tuberculosis treatment: preparation and characterization of particles. AAPS PharmSciTech 2010;11(2):538–49.
[46] Maria Leena M, Gover Antoniraj M, Moses JA, Anandharamakrishnan C. Three fluid nozzle spray drying for co-encapsulation and controlled release of curcumin and resveratrol. J Drug Deliv Sci Technol 2020;57:101678.
[47] Shi X, Lee Y. Encapsulation of tributyrin with whey protein isolate (WPI) by spray-drying with a three-fluid nozzle. J Food Eng 2020;281(Suppl 2):109992.
[48] Kondo K, Niwa T, Danjo K. Preparation of sustained-release coated particles by novel microencapsulation method using three-fluid nozzle spray drying technique. Eur J Pharm Sci 2014;51:11–9.
[49] Stöber W, Fink A, Bohn E. Controlled growth of monodisperse silica spheres in the micron size range. J Colloid Interface Sci 1968;26(1):62–9.
[50] Xia Y, Zhang C, Wang JX, Wang D, Zeng XF, Chen JF. Synthesis of transparent aqueous ZrO_2 nanodispersion with a controllable crystalline phase without modification for a high-refractive-index nanocomposite film. Langmuir 2018;34(23):6806–13.
[51] Yang DL, Sun Q, Niu H, Wang RL, Wang D, Wang JX. The properties of dental resin composites reinforced with silica colloidal nanoparticle clusters: effects of heat treatment and filler composition. Compos Part B Eng 2020;186:107791.
[52] Nagashima S, Yoshida A, Ansai T, Watari H, Notomi T, Maki K, et al. Rapid detection of the cariogenic pathogens *Streptococcus mutans* and *Streptococcus sobrinus* using loop-mediated isothermal amplification. Oral Microbiol Immunol 2007;22(6):361–8.
[53] Bürgers R, Eidt A, Frankenberger R, Rosentritt M, Schweikl H, Handel G, et al. The anti-adherence activity and bactericidal effect of microparticulate silver additives in composite resin materials. Arch Oral Biol 2009;54(6):595–601.
[54] Burke FJT, Crisp RJ, Bell TJ, Healy A, Mark B, McBirnie R, et al. One-year retrospective clinical evaluation of hybrid composite restorations placed in United Kingdom general practices. Quintessence Int 2001;32(4):293–8.
[55] Zalkind MM, Keisar O, Ever-Hadani P, Grinberg R, Sela MN. Accumulation of *Streptococcus mutans* on light-cured composites and amalgam: an *in vitro* study. J Esthet Dent 1998;10(4):187–90.